

# Discrete self-similarity in thin films with van der Waals interactions and the formation of iterated structures

Michael C. Dallaston<sup>1</sup>, Marco A. Fontelos<sup>2</sup>, Dmitri Tseluiko<sup>3</sup>, Serafim Kalliadasis<sup>1\*</sup>

<sup>1</sup>*Department of Chemical Engineering,  
Imperial College London,  
London SW7 2AZ, UK*

<sup>2</sup>*Instituto de Ciencias Matemáticas,  
C/Nicolás Cabrera, Madrid, 28049, Spain*

<sup>3</sup>*Department of Mathematical Sciences,  
Loughborough University,  
Loughborough LE11 3TU, UK*

The formation of iterated structures, such as satellite and sub-satellite drops, filaments, bubbles, etc is a common phenomenon in free surface flows. We provide a computational and theoretical study of the origin of these patterns in the case of thin films of viscous fluids subject to long-range molecular forces. Iterated structures appear as a consequence of discrete self-similarity, where patterns repeat themselves, subject to rescaling, periodically in a logarithmic time scale. The result is an infinite sequence of ridges and filaments with similarity properties. The character of these discretely self-similar solutions as the result of a Hopf bifurcation from ordinarily self-similar solutions is also described.

Free surface flows can produce a great diversity of patterns such as filaments, drops, bubbles, waves, etc (see [1] for a review). Among them, probably the most intriguing and elusive to analyze have been the so called “iterated patterns”, where the same structure repeats itself at different times and length scales. Examples are the formation of several generations of satellite drops in capillary breakup [2], the cascade of structures (filaments) produced in very viscous jets [3], [4] and the iterated stretching of viscoelastic filaments [5], [6]. In this letter, we present for the first time a scenario in which a rigorous analysis reveals how such structures may appear as a bifurcation, as some structural parameter changes, from self-similar solutions to discretely self-similar solutions (see [7] for a general review) where scale invariance occurs only at discrete times, resulting in the infinite repetition of some pattern at a discrete sequence of time and length scales.

The physical situation we consider is the rupture of thin films driven by long range molecular forces. The forces are derived from a van der Waals-type potential. When the singularity in the potential at zero thickness is sufficiently weak, a transition between ordinary self-similarity and discrete self-similarity takes place and film rupture occurs after an infinite sequence of droplets is produced.

Thin liquid films are ubiquitous in a wide spectrum of natural phenomena and technological applications [8]. When the film thickness is sufficiently small, molecular forces play an important role and may cause the film to destabilize and eventually rupture and dewet the substrate. Under the assumption of a thin film, the problem may be formulated in terms of an evolution equation for the film profile  $h(\mathbf{x}, t)$  in the form  $h_t = -\nabla \cdot \mathbf{q}$ , where  $\mathbf{q} = -(h^3/3\mu)\nabla p$  is the flow rate, with  $\mu$  being the fluid’s

viscosity, and the pressure  $p$  has two contributions:

$$-p = \sigma \nabla^2 h + \Pi(h).$$

The first component is the Laplace pressure (linearized curvature times surface tension coefficient) and the second is the disjoining pressure taken to be of the form

$$\Pi(h) = -\frac{A}{h^n}.$$

In one spatial dimension, and after a suitable nondimensionalization, the model for the evolution of a thin liquid film under the action of molecular forces then reads

$$h_t + \left[ h^3 \left( h_{xx} - \frac{1}{nh^n} \right) \right]_x = 0. \quad (1)$$

In the context of rupture by van der Waals forces,  $A$  (strictly,  $6\pi A$ ) is the Hamaker constant, while the exponent is almost always taken to be  $n = 3$  [9–11]. At this value, the remarkable property of solutions of (1) is the development of self-similar film rupture ( $h = 0$  at a single point) in finite time. There is, however, good reason to examine different values of  $n$ . Firstly, different intermolecular forces can result in different exponents, for instance,  $n = 1$  for hydrogen bonds or  $n = 2$  for surface charge-dipole interactions [12]. Secondly, as well as intermolecular forces, the above formulation is also used to model other thin-film phenomena at different scales, such as destabilization of thin films due to thermocapillarity [13–15] and density contrast (Rayleigh–Taylor instability) [16]; in such cases we may define an equivalent “disjoining pressure”, which behaves as  $\Pi(h) \sim \ln(h)$  for the thermocapillary effect (essentially  $n = 0$ ), or  $\Pi(h) \sim h$  for the Rayleigh–Taylor instability ( $n = -1$ ). Instead of self-similar rupture, these two examples exhibit cascades of satellite droplets, similar to those discussed above, so

it is of great interest to understand how the two behaviors are connected through variation in  $n$ .

Assuming that rupture occurs at a single point  $x_0$  and at time  $t_0$ , it is natural to seek solutions in a self-similar form:

$$h(x, t) = (t_0 - t)^\alpha f\left(\xi \equiv \frac{x - x_0}{(t_0 - t)^\beta}\right), \quad (2)$$

where, from simple dimensional arguments based on (1), one finds the following values for the similarity exponents  $\alpha$  and  $\beta$ :

$$\alpha = \frac{1}{2n-1}, \quad \beta = \frac{n+1}{4n-2} \quad (3)$$

In order for a self-similar solution representing rupture to exist, we must assume  $n > 1/2$ , so that  $\alpha$  and  $\beta$  are positive. The self-similar solution  $f(\xi)$  must then satisfy the equation

$$-\frac{1}{2n-1}f + \frac{n+1}{4n-2}\xi f_\xi + \left[f^3\left(f_{\xi\xi} - \frac{1}{nf^n}\right)\right]_\xi = 0, \quad (4)$$

subject to the condition that the interface profile  $h(x, t)$  remains finite at a finite distance from  $x_0$ . As  $t \rightarrow t_0$ , one has  $\xi \rightarrow \infty$  and, in order to cancel out any dependence on  $t_0 - t$  we must impose

$$f(\xi) \sim C_\pm |\xi|^{\alpha/\beta} = C_\pm |\xi|^{2/(n+1)} \text{ as } |\xi| \rightarrow \infty, \quad (5)$$

where  $C_\pm$  are constants as  $\xi \rightarrow \pm\infty$ .

Above a certain value of  $n$ , there are an infinite number of solutions to (2) with boundary condition (5). This fact was established for the particular case  $n = 3$  in [9] and was recently extended to general  $n$  by the authors [17]. These solutions are symmetric, that is,  $C_+ = C_-$ , and can be arranged (for a given value of  $n$ ) as a sequence  $f_1, f_2, f_3, \dots$  according to their values at  $\xi = 0$  such that  $f_1(0) > f_2(0) > \dots$ . We can thus depict solution branches as  $f_j(0)$  over  $n$ , as in Fig. 1. These solutions were computed using the open source numerical continuation software AUTO-07p [18] (see also [17, 19]). As  $n$  is decreased, the solution branches merge, with the first two branches merging at the critical value  $n_c = 1.49915$  [17]. Our focus in this letter is on the change in dynamics of solutions to (1) close to this value.

To compute numerical solutions to (1), we implement an adaptive finite difference scheme that increases local mesh refinement near the minimum of  $h$  whenever  $h_{\min}$  is less than half of its value at the previous mesh refinement. In Fig. 2, we represent the result of such a computation with  $n = 1.7$ , as well as a comparison of the numerical profiles rescaled according to (2) with the self-similar solution  $f_1(\xi)$ . At this value of  $n$ , the solution ruptures in finite time  $t_0$ . If we solve (1) with  $n = 1.4$  instead (Fig. 3), the situation changes dramatically; there is still finite-time rupture at a single point, but the approach is

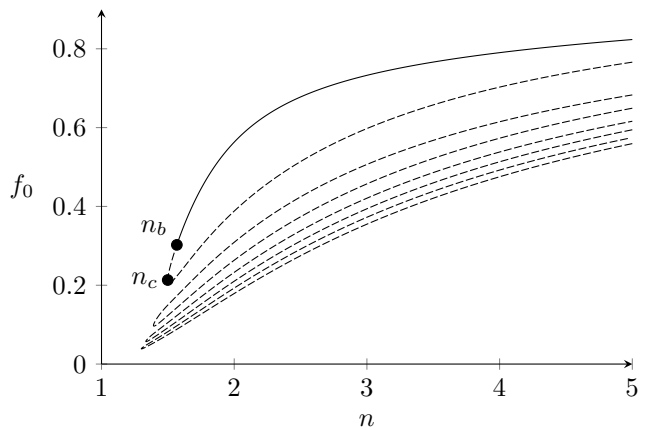


FIG. 1. Bifurcation diagram for self-similar solutions  $f(\xi)$  satisfying (4), labelled by their value at the origin  $f_0 = f(0)$ . For sufficiently large  $n$ , there are infinitely many solutions. At  $n = n_c \simeq 1.49915$  there is a first turning point where the first and second branches of solutions merge. Successive turning points exist at 1.39141, 1.33405, 1.29993,  $\dots$ . The primary branch is stable for most of its domain; however, as we describe in this letter, it becomes unstable below  $n = n_b$  due to a Hopf bifurcation there (see Fig. 5).

not in the form (2) anymore, with the solution instead developing an infinite cascade of satellites of decreasing size at  $x > x_0$  and at  $x < x_0$ .

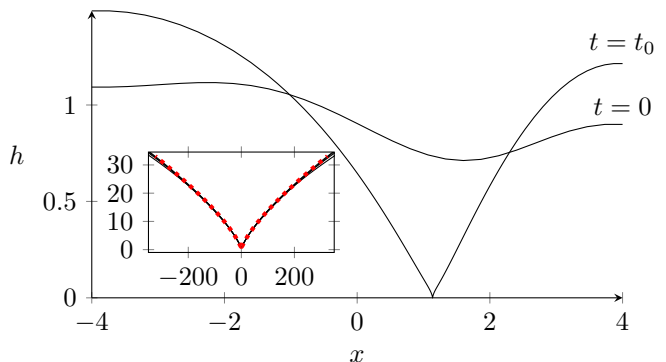


FIG. 2. Evolution towards rupture in the domain  $[-L, L]$ ,  $L = 4$ , with the initial profile  $h(x, 0) = 1 - (1/10)\cos(\pi x/2L) - (1/5)\sin(\pi x/L)$  and  $n = 1.7$ . Rupture occurs at a point at time  $t = t_0$ . Inset: Interface profiles near the singularity rescaled according to (2), and comparison with the stable self-similar solution (dotted line). Notice that the interface profiles approach a symmetric self-similar shape, although the initial profile is asymmetric.

The existence of these spatial and temporal oscillations at  $n = 1.4$  indicates discretely self-similar (DSS) solutions (see [20], [21] for a general reference on DSS and its role in various physical systems). For these solutions, the relationship (2) holds only for a discrete family of times  $t_1, t_2, \dots$ , which approach  $t_0$  exponentially. As argued in [7], DSS solutions appear as periodic orbits when writing

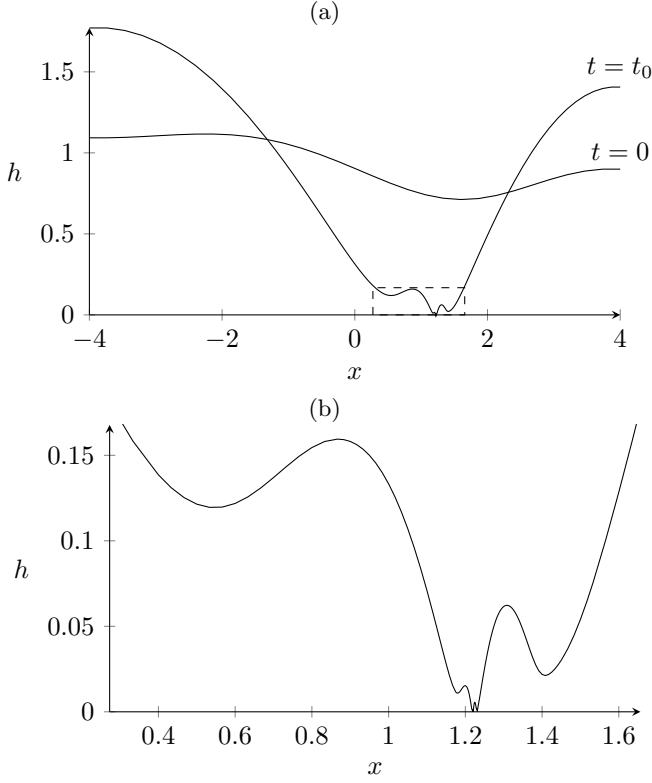


FIG. 3. (a) Evolution towards rupture in the domain  $[-L, L]$ ,  $L = 4$ , with the initial profile  $h(x, 0) = 1 - (1/10)\cos(\pi x/2L) - (1/5)\sin(\pi x/L)$  and  $n = 1.4$ . Rupture occurs at a point at time  $t = t_0$ . In this case, the evolution does not appear to be of the classical self-similar type. (b) The region near the singularity.

(2) in the natural self-similar variables. More precisely, we perform the change of variables:

$$h(x, t) = (t_0 - t)^\alpha F\left(\tau = -\log(t_0 - t), \xi \equiv \frac{x - x_0}{(t_0 - t)^\beta}\right) \quad (6)$$

so that (1) with  $\alpha, \beta$  given by (3) transforms into the equation:

$$F_\tau - \frac{1}{2n-1}F + \frac{n+1}{4n-2}\xi F_\xi + \left[F^3\left(F_{\xi\xi} - \frac{1}{nF^n}\right)\right]_\xi = 0, \quad (7)$$

The scaled time variable  $\tau$  tends to infinity as  $t \rightarrow t_0$ . Self-similar solutions  $f_1, f_2, \dots$  of (4) are fixed (or equilibrium) points (that is,  $\tau$ -independent) of (7) viewed as a dynamical system in the scaled time  $\tau$ . Hence, for a given value of  $n$ ,  $F(\tau, \xi) = \{f_1(\xi), f_2(\xi), f_3(\xi), \dots\}$  is the set of equilibrium points in the dynamics. Besides equilibrium points, other attractors such as periodic orbits may be present. A periodic orbit of period  $T$  is characterized by the property  $F(\tau + T, \xi) = F(\tau, \xi)$  for any value of  $\tau$ . Thus, the same profile  $(x - x_0, h)$ , up to rescaling both coordinates with  $(t_0 - t)^\beta$  and  $(t_0 - t)^\alpha$  respectively, will

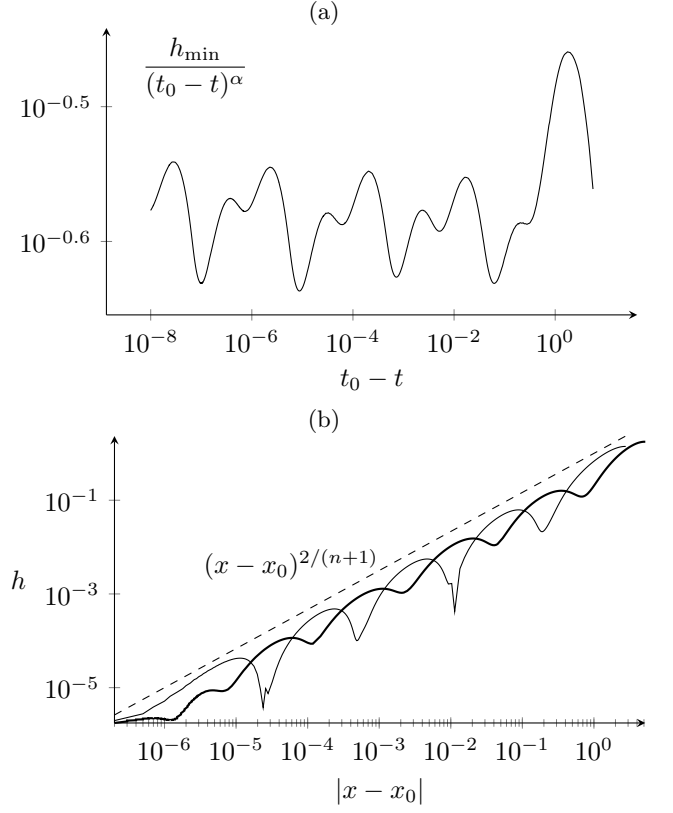


FIG. 4. (a) Logarithmic plot of the minimum interface height  $h_{\min}$  divided by the assumed similarity scaling  $(t_0 - t)^\alpha$ , against time to the singularity  $t_0 - t$ . On average,  $h_{\min}$  is dictated by the scaling, but also exhibits periodic oscillations that are characteristic of discrete self-similarity. We have computed four complete periods. (b) Logarithmic plot of the interface shape against distance to the point of rupture  $x_0$  close to time  $t_0$ . The two branches correspond to  $x > x_0$  (unbolded line) and  $x < x_0$  (bolded line). On average, the slope is dictated by scaling (dashed line), but large periodic oscillations are observed, corresponding to sequences of ridges and necks.

appear at times  $t_1, t_2, \dots, t_N, \dots$  such that

$$\frac{t_0 - t_{N+1}}{t_0 - t_N} = e^{-T}. \quad (8)$$

From our numerical observation of the evolution of (1) for  $n = 1.7$  in Fig. 2, and  $n = 1.4$  in Fig. 3, it is clear that the nature of the self-similarity changes significantly between these two values. We will now argue that attracting periodic orbits occur when  $n$  is smaller than a critical value  $n_b \simeq 1.576$ , strictly larger than the value  $n_c$  at which the first two branches merge.

As the first evidence for a periodic behavior, in Fig. 4 we represent the evolution of the minimum interface height  $h_{\min}(t)$  in a logarithmic scale for a full numerical simulation of (2) with  $n = 1.4$ . In the case of a self-similar solution in the form (2), one would have  $h_{\min} \sim f_0(t_0 - t)^\alpha$ . In the case of a DSS solution, the minimum in

$\xi$  of  $F$  is achieved at a point  $\xi_0(\tau)$  changing periodically in  $\tau$ , and hence we have  $h_{\min} = F(\tau, \xi_0(\tau))(t_0 - t)^{-\alpha}$ . On a logarithmic scale this relation is a superposition of a straight line of slope  $-\alpha$  and a periodic function in  $\tau$ . In Fig. 4 we plot  $h_{\min}$  divided by  $(t_0 - t)^\alpha$  against  $t_0 - t$  on a logarithmic scale. The periodicity can be clearly seen, and we resolve  $h_{\min}$  down to  $10^{-8}$ , which covers four full periods. From these numerics we estimate the period to be  $T \simeq 4.6$ .

Secondly, in Fig. 4b we plot  $h$  against  $|x - x_0|$ , on a logarithmic scale, for  $t$  very close to  $t_0$ . In the case of self-similar rupture, the far field condition of  $f$  (5) sets the power law behaviour of the film profile near rupture to be  $h \sim C_\pm |x - x_0|^{2/(n+1)}$ . For a DSS solution, the far field of  $f$  oscillates in scaled time  $\tau$ , which leaves behind a pattern of local maxima and minima, whose amplitude and spacing decreases exponentially as the rupture point  $x_0$  is approached. The local maxima can be interpreted as tops of “drops” and the local minima as necks separating the drops. The maxima  $h_1, h_2, \dots, h_N, \dots$  are located at distances  $d_1, d_2, \dots, d_N, \dots$  from  $x_0$ . The distances  $d_i$  correspond to identical values of  $\xi = d_i(t_0 - t_i)^{-\beta}$  and the heights  $h_i$  correspond to identical values of  $f = h_i(t_0 - t_i)^{-\alpha}$ , at times  $t_i$  satisfying (8). Hence, from (6) we deduce

$$\frac{d_N}{d_{N+1}} = e^{\beta T}, \quad \frac{h_N}{h_{N+1}} = e^{\alpha T}.$$

These predicted values are accurately reflected in the numerical result in Fig. 4.

A theoretical understanding of self-similar dynamics requires the computation of not only the equilibrium points but also their stability. For  $n = 3$  it has been shown [10, 11] that besides two trivial eigenvalues that correspond to space and time translation of the singularity [7], all eigenvalues of the linearization of (7) about  $f_1(\xi)$  are negative. Hence, the similarity solution  $f_1(\xi)$  is a stable equilibrium point.  $f_2(\xi)$ , on the other hand, has one positive nontrivial eigenvalue and  $f_3(\xi)$  has two nontrivial eigenvalues, etc. All equilibrium points other than  $f_1(\xi)$  are therefore unstable.

We now compute the stability of  $f_1(\xi)$  as  $n$  varies. This is again carried out using AUTO-07p [18]. We linearize equation (7) about  $f_1(\xi)$  and seek solutions of the linearized problem of the form  $\tilde{f}(\tau, \xi) = e^{\sigma\tau}\Phi(\xi)$ , which leads to an eigenvalue problem for  $\sigma$ . For complex eigenvalues we will write  $\sigma = \sigma_R + i\sigma_I$ .

The four eigenvalues  $\{\sigma_j\}$  with largest real part are represented in Fig. 5. The largest is  $\sigma_1 = 1$ , which is the trivial eigenvalue corresponding to changes in  $t_0$  (the eigenvalue arising from a perturbation in  $x_0$  is suppressed by the assumed symmetry). The pair  $\sigma_{2,3}$  are complex conjugates that result from the collision of two real eigenvalues at a point  $n > 5$ . At a critical value  $n = n_b \simeq 1.567 > n_c$ , the real part  $\sigma_{R2,3}$  of this complex

pair crosses from negative to positive; hence, as  $n$  decreases, the stable focus  $f_1(\xi)$  switches into an unstable focus which results in a periodic orbit via a Hopf bifurcation. The imaginary part of the eigenvalue  $\sigma_{I2,3}$  at  $n = n_b$  sets the frequency of oscillations of the periodic orbits as  $n \rightarrow n_b^-$  and of damped oscillations about  $f_1(\xi)$  as  $n \rightarrow n_b^+$ . We find this value to be  $\sigma_I \simeq \pm 0.9125$ .

Finally,  $\sigma_4$  is the largest nontrivial real eigenvalue. It plays a role in the fold bifurcation at  $n = n_c$ , where the first and second branches merge. In Fig. 5b we zoom in on the bifurcation structure near the fold. The picture is complicated by the return of  $\sigma_{2,3}$  to the real plane just above the fold; one eigenvalue ( $\sigma_2$ , say) decreases, and appears to collide with  $\sigma_4$ , very close ( $\sigma_R = O(10^{-2})$ ) to zero. This implies the fold is either at or very close to a Bogdanov–Takens (double zero) bifurcation [22]. On the second branch, the double eigenvalue continues as a complex conjugate pair (depicted as a dashed line in the figure). The second eigenvalue ( $\sigma_3$ ) increases as the fold is approached and collides with  $\sigma_1$ ; its continuation to the second branch is also depicted as a dashed line in Fig. 5.

A natural question is whether further bifurcations take place at smaller values of  $n$ , leading to more complicated dynamics. We considered the particular case  $n = 0.7$  which is far from  $n_c$  but still above  $n = 1/2$ . As we can see in Fig. 6, the minimum height roughly evolves according to the similarity scaling, but the oscillation around the similarity exponent does not show any periodicity. This translates into a distribution of drops near  $t = t_0$  without any clear pattern.

Finally we note that previous studies on thermocapillary and Rayleigh–Taylor instability [13, 16], which have equivalent disjoining pressures with values  $n < 1/2$ , show that the formation of smaller and smaller drops occurs through a process that appears chaotic, and this behavior is also exhibited when the system is modeled with the full Stokes or Navier–Stokes equations [13, 15]. The transition from finite-time self-similar rupture to DSS, and then to chaotic behavior, is therefore of true physical interest in the study of thin-film phenomena and is worth further theoretical investigation.

---

\* MCD and MAF contributed equally to this study and the preparation of the manuscript. MCD was supported by the EPSRC under grant no. EP/K008595/1.

- [1] Eggers, J., Villermaux, E. Physics of liquid jets. Rep. Prog. Phys. 71 (2008): 1–79.
- [2] Tjahjadi M., Stone H. A. and Ottino J. M., Satellite and subsatellite formation in capillary breakup, J. Fluid Mech., 243 (1992), 297–317.
- [3] X. D. Shi, M. P. Brenner, S. R. Nagel, A cascade of structure in a drop falling from a faucet, Science 265, 219–222 (1994).

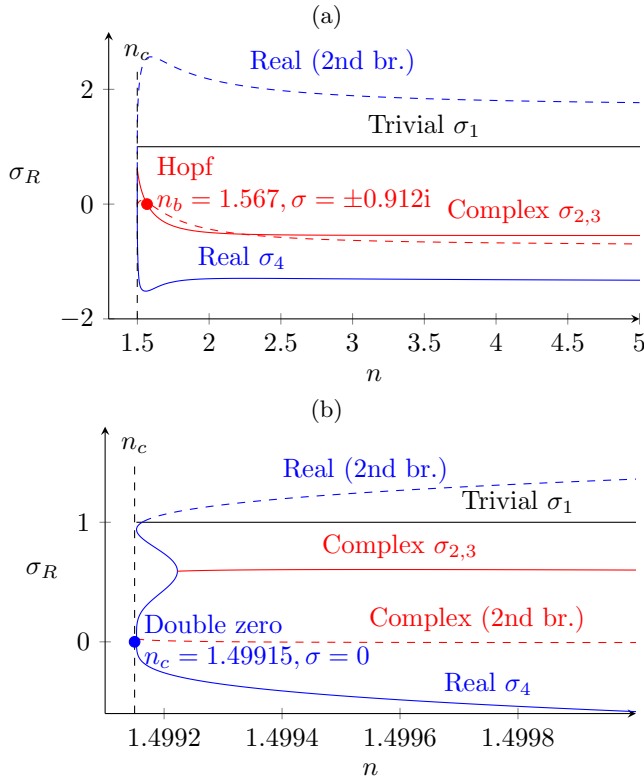


FIG. 5. (a) The real part  $\sigma_R$  of eigenvalues governing the stability of the primary solution branch  $f_1(\xi)$  as  $n$  varies (solid), and eigenvalues of the second branch  $f_2(\xi)$  (dashed). The real part of the complex eigenvalues  $\sigma_{2,3}$  crosses zero at  $n_b \simeq 1.567$ , indicating a Hopf bifurcation. (b) The eigenvalues near the point at which the two solution branches  $f_1(\xi)$  and  $f_2(\xi)$  merge. These results suggest the system exhibits or is very close to a Bogdanov–Takens (double zero) bifurcation at  $n = n_c$ .

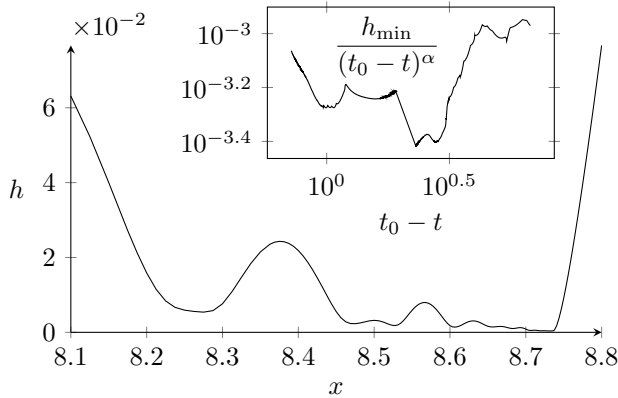


FIG. 6. Interface profile for  $n = 0.7$  and  $t$  close to  $t_0$ . No regular pattern can be observed. Inset: logarithmic plot of the minimum height, divided by the appropriate similarity scaling, against time to the singularity. Note the apparent chaos without a clearly defined pattern.

[4] M. P. Brenner, X. D. Shi and S. R. Nagel, Iterated instabilities during droplet fission, *Phys. Rev. Lett.* 73, 3391 (1994).

- [5] H. C. Chang, E. A. Demekhin, and E. Kalaidin, Iterated stretching of viscoelastic jets, *Phys. Fluids* 11, 1717 (1999).
- [6] Oliveira, M. S. N. & McKinley, G. H. Iterated stretching and multiple breads-on-a-string phenomena in dilute solutions of highly extensible flexible polymers. *Phys. Fluids* 17, 071704 (2005).
- [7] J. Eggers, M. A. Fontelos, *Singularities: Formation, Structure, and Propagation*, Cambridge University Press, 2015.
- [8] R. V. Craster and O. K. Matar, Dynamics and stability of thin liquid films, *Rev. Mod. Phys.*, 81 (2009), pp. 1131–1198.
- [9] W. W. Zhang and J. R. Lister, Similarity solutions for van der Waals rupture of a thin film on a solid substrate, *Phys. Fluids* 11 (1999), 2454.
- [10] T. P. Witelski, A. J. Bernoff, Stability of self-similar solutions for van der Waals driven thin film rupture, *Phys. Fluids*, 11 (1999), 2443–2445.
- [11] T. P. Witelski, A. J. Bernoff, Dynamics of three-dimensional thin film rupture, *Physica D*, 147 (2000), 155–176.
- [12] G. F. Teletzke, H. T. Davis, L. E. Scriven, How liquids spread on solids, *Chem. Eng. Commun.*, 55 (1987), 41–82.
- [13] W. Boos and A. Thess, Cascade of structures in long-wavelength Marangoni instability, *Phys. Fluids*, 11 (1999), 1484–1494.
- [14] A. Alexeev, T. Gambaryan-Roisman, P. Stephan, Marangoni convection and heat transfer in thin liquid films on heated walls with topography: Experiments and numerical study, *Phys. Fluids*, 17 (2005), 062106.
- [15] S. Krishnamoorthy, B. Ramaswamy and S. W. Joo, Spontaneous rupture of thin liquid films due to thermocapillarity: A full-scale direct numerical experiment, *Phys. Fluids*, 26 (2014), 072001.
- [16] S. G. Yiantsios, B. G. Higgins, Rayleigh–Taylor instability in thin viscous films, *Phys. Fluids A*, 1 (1989), 1484–1501.
- [17] M. C. Dallaston, D. Tseluiko, S. Kalliadasis, M. A. Fontelos, Z. Zheng, Self-similar finite-time singularity formation in degenerate parabolic equations arising in thin-film flows, Preprint 2016.
- [18] E. J. Doedel, A. R. Champneys, F. Dercole, T. F. Fairgrieve, Y. A. Kuznetsov, B. Oldeman, R. C. Paffenroth, B. Sandstedt, X. J. Wang, C. H. Zhang, AUTO-07p, Continuation and bifurcation software for ordinary differential equations, (2007), <http://indy.cs.concordia.ca/auto/>.
- [19] D. Tseluiko, J. Baxter, U. Thiele, A homotopy continuation approach for analysing finite-time singularities in thin liquid films, *IMA J. Appl. Math.*, 78 (2013), 762–776.
- [20] D. Sornette, Discrete-scale invariance and complex dimensions, *Physics reports* 297 (5) (1998), 239–270.
- [21] D. Sornette, *Critical Phenomena in Natural Sciences: Chaos, Fractals, Self-Organization and Disorder: Concepts and Tools*, Springer Science & Business Media 2006.
- [22] Y. A. Kuznetsov, *Elements of Applied Bifurcation Theory*, Vol.112, Springer Science & Business Media 2013.